Magnetism of Ho_{1−x}Tb_{x}Al_{2} alloys: Critical dependence of a first-order transition on Tb concentration

Mahmud Khan, Ya. Mudryk, K. A. Gschneidner, Jr., and V. K. Pecharsky

Phys. Rev. B **84**, 214437 — Published 27 December 2011

DOI: 10.1103/PhysRevB.84.214437

Magnetism of $Ho_{1-x}Tb_xAl_2$ alloys: Critical dependence of a first order transition on Tb concentration

Mahmud Khan, Ya. Mudryk

The Ames Laboratory, U.S. Department of Energy, Iowa State University, Ames, Iowa 50011-3020, USA

K. A. Gschneidner, Jr. and V. K. Pecharsky

The Ames Laboratory, U.S. Department of Energy, Iowa State University, Ames, Iowa 50011-3020, USA, and

Department of Materials Science and Engineering, Iowa State University, Ames, Iowa 50011-2300, USA

$HoAl_2$ exhibits a first order spin reorientation transition at 20 K, which is manifested as a sharp peak in the heat capacity. When Ho is partially replaced by only five percent of Tb, the sharp heat capacity peak in $Ho_{1-x}Tb_xAl_2$ (x= 0.05) disappears, and then reappears again for $x \geq 0.07$. For x = 0.05, the anomaly corresponding to the spin reorientation transition is barely seen in the heat capacity, but as x exceeds 0.07 the weak anomaly transforms to a sharp peak. The spin reorientation transition temperature increases to 29 K for x = 0.05, and as x increases further the transition shifts to lower temperature and returns to ~20 K for x = 0.25. The transition is no longer observed when x exceeds 0.60. Temperature dependent x-ray powder diffraction data confirm the first order nature of the spin reorientation transition for the alloy with x = 0.40, and indicate that the compound retains the room temperature cubic structure within the sensitivity of the technique.

Experimental observations are discussed considering the easy magnetization directions of $HoAl_2$ and $TbAl_2$

PACS No.'s: 75.30.Gw, 75.10.Dg, 75.30.Sg

INTRODUCTION

The rare earth elements (lanthanides) are generally divided into two groups. The light lanthanides are the ones with atomic numbers 57 (lanthanum) through 63 (europium) and the heavy lanthanides are the ones with atomic numbers 64 (gadolinium) through 71 (lutetium). Each of these two groups may be further divided into two subgroups based on the signs of their respective second order Stevens' factors α_J,[1] which represent the shapes of the angular distribution of the *4f* electron charge densities of the elements. The shape is an oblate spheroid when $\alpha_J < 0$ or a prolate spheroid when $\alpha_J > 0$.[2]

Recent studies showed that when two lanthanides with *4f* electron charge densities of different shape are mixed together in pseudo-binary $R_{1-x}R'_xAl_2$ compounds (R and R' are lanthanide metals where R has a positive second order Stevens' factor and the same for R' is negative), interesting magnetic phenomena are observed.[3,4,5,6,7] For certain critical concentrations centered at $x = 0.25$, sharp peaks, representing first order phase transitions, are observed in the heat capacity, C_P, data of the $R_{1-x}R'_xAl_2$ alloys. The peaks are suppressed upon the application of weak magnetic fields. The nature of the peaks appears to depend on both the signs and magnitudes of the second order Stevens' factors of the different lanthanides present in the $R_{1-x}R'_xAl_2$ system.

While the second order Stevens' factors represent the shapes of the 4*f* charge density distributions of R, the fourth and sixth order Stevens' factors (β and γ, respectively) are related to the anisotropy of R. In certain lanthanide alloys competition between β and γ

results in first order spin reorientation transitions.[8] Among binary dialuminides, RAl_2, holmium dialuminides, $HoAl_2$, is the only compound that exhibits a sharp first order peak in its C_P data. The sharp peak occurs at $T_{SR} \cong 20$ K due to a temperature induced first order spin reorientation transition, during which the easy axis of ferromagnetic $HoAl_2$ changes from [110] direction (below 20 K) to [100] direction (above 20 K). Magnetization,[9,10,11] magnetic-torque,[12,13] specific heat,[14,15,16] and neutron scattering measurements[17] have been used to explore this property of $HoAl_2$. Shankar *et al*. calculated the temperature dependence of the free energy of $HoAl_2$ for Ho in $HoAl_2$ considering the exchange field (H_{ex}) directed along the three major directions.[18] It was shown that the free energy was lowest with H_{ex} along the [110] direction below 20 K, and above 20 K the lowest value of the free energy is with H_{ex} along the [100] direction. The free energies are significantly dependent on the fourth and sixth order Stevens' factors, which are both negative for Ho. If Ho in $HoAl_2$ is partially replaced by another R atom with different Stevens' factors, the nature of the spin reorientation transition is expected to change significantly.

In this paper we report an experimental study performed on a series of $Ho_{1-x}Tb_xAl_2$ alloys probing the effect of partially replacing Ho by Tb on the spin reorientation transition of $HoAl_2$. Since the magnitudes of the Stevens' factors, along with the signs of β, are different for Ho and Tb, interesting behaviors related to the first order spin reorientation transition are expected to be observed in $Ho_{1-x}Tb_xAl_2$ alloys. In order to explore such behavior, we have performed heat capacity measurements on a series of $Ho_{1-x}Tb_xAl_2$

alloys in zero and non-zero magnetic fields, and temperature-dependent x-ray powder diffraction measurements on a representative alloy with x = 0.4.

EXPERIMENTAL DETAILS

The $Ho_{1-x}Tb_xAl_2$ ($0 \leq x \leq 0.75$) alloys weighing approximately 5 g each were prepared by conventional arc melting in an argon atmosphere. The Ho and Tb metals used in the preparation were 99.8+ at. % (99.98 wt %) pure with respect to all other elements in the periodic table, and were obtained from the Materials Preparation Center of the Ames Laboratory.[19] The Al metal of 5N purity was purchased from Alfa Aesar Inc. The alloys melt congruently, and therefore, annealing was not necessary. The phase purities of the samples were checked by performing room temperature x-ray powder diffraction (XRD) on a PANAnalytical powder diffractometer employing monochromatic Cu $K_{\alpha 1}$ radiation. The crystal structure and the lattice parameters were determined by performing Reitveld refinement using LHPM Rietica.[20] The XRD patterns along with the Reitveld refinements show that each alloy is single phase (within the accuracy of the technique that is ~1 vol.% of an impurity phase[21]) and crystallizes in the $MgCu_2$ C15 type cubic Laves phase structure. Temperature dependent XRD measurements were performed on a Rigaku TTRAX rotating anode powder diffractometer employing Mo Kα radiation.[22] The diffractometer was equipped with a continuous flow ^{4}He cryostat controlling the temperature of the sample, which was prepared and mounted on a copper sample holder as described in Ref.23.

The heat capacity measurements were conducted using a homemade adiabatic heat-pulse calorimeter.[24] The measurements were performed in the temperature range from ~3.8 to 300 K in zero magnetic field and in applied magnetic fields up to 30 kOe. The errors in the heat capacity measurements were less than 0.7%. Magnetization measurements were conducted using a Superconducting Quantum Interference Device (SQUID) magnetometer MPMS XL-7 manufactured by Quantum Design Inc.

RESULTS AND DISCUSSION

The heat capacities, C_P, of $Ho_{1-x}Tb_xAl_2$ ($0 \leq x \leq 0.1$) measured in zero magnetic field are shown in Fig. 1. As shown in Fig. 1a, the C_P of the alloy with x = 0 (i.e. pure $HoAl_2$) exhibits a sharp peak at $T_{SR} \cong 20$ K, representing the first order spin reorientation transition, and a lambda type peak at $T_C \cong 32$ K that represents the ferromagnetic transition. These behaviors are consistent with earlier reports. [14,16] Remarkable changes are observed in Fig.1b through Fig.1d. As Ho is replaced by only 5% Tb in $Ho_{1-x}Tb_xAl_2$, the first order spin reorientation peak is no longer observed in the C_P data (see Fig. 1b). Instead, a weak anomaly occurs at ~29 K, more clearly seen in the derivative of the C_P data of the alloy with x = 0.05 (see inset of Fig. 1b). As the Tb concentration is increased to 7%, the weak anomaly develops into a minor peak in the C_P data of the $Ho_{1-x}Tb_xAl_2$ (x = 0.07) alloy (see Fig. 1c). The peak is more pronounced and sharper in the C_P data of the alloy with x = 0.10 (see Fig. 1d).

Figure 2 shows the zero magnetic field C_P data of the $Ho_{1-x}Tb_xAl_2$ ($0.15 \leq x \leq 0.75$) alloys. As shown in Fig. 2, the sharp peak becomes more prominent as x changes from 0.15 to 0.4, and then weakens for x = 0.5 and 0.6, finally disappearing when x = 0.75. It is interesting to note, that for the alloy with x = 0.25 the C_P anomaly is nearly identical to the anomaly observed in the C_P of pure $HoAl_2$ in the vicinity of the first order spin reorientation transition (compare Fig.1a with Fig. 2b). Even the temperatures at which the sharp peaks appear are almost identical in the two samples (20.1 K for $HoAl_2$ and 20.4 K for the $Ho_{1-x}Tb_xAl_2$ alloy with x = 0.25).

Considering apparent similarity of the sharp heat capacity peaks, it is highly probable that similar to $HoAl_2$, the first order anomalies observed in the $Ho_{1-x}Tb_xAl_2$ alloys are related to spin reorientation transitions. It also follows from the experimental data presented above that the interactions responsible for the spin reorientation transition in $HoAl_2$ are significantly weakened when even a small amount of Tb is added in $Ho_{1-x}Tb_xAl_2$. This weakening causes the disappearance of the first order peak in the $Ho_{1-x}Tb_xAl_2$ alloy with x = 0.05. However, further Tb additions result in modified interactions in the $Ho_{1-x}Tb_xAl_2$ system which are represented as the weak anomaly observed in the alloy with x = 0.05 (see Fig. 1b). With increasing Tb concentration the interactions become stronger, and hence the anomaly in the C_P data of the $Ho_{1-x}Tb_xAl_2$ alloys becomes stronger (see Fig.1 and Fig.2). For $x \geq 0.10$ the C_P anomaly becomes quite sharp and clearly represents a first order phase transition. As x exceeds 0.40, the interactions responsible for the first order anomalies observed in $Ho_{1-x}Tb_xAl_2$ start to weaken, and eventually fade away. As a result, no anomaly is observed in the C_P data of the $Ho_{1-x}Tb_xAl_2$ alloys with $x > 0.6$.

The above described anomalies may be discussed by considering the easy magnetization directions (anisotropies) of $HoAl_2$ and $TbAl_2$, which are [111] for $TbAl_2$ at all temperatures and [110] (below 20 K) and [100] (above 20 K) for $HoAl_2$. The easy direction of magnetization at any given temperature corresponds to the state with the lowest free energy.[18] In $HoAl_2$, the free energy is lowest with H_{ex} along the [110] direction below 20 K and the energy becomes lowest with H_{ex} along the [100] direction at and above 20 K. The free energies are dependent on the fourth and sixth order Stevens factors, which are different in magnitude and sign for Ho^{3+} and Tb^{3+}. Therefore, the free energy landscape is expected to change significantly as Ho is partially replaced by Tb in $Ho_{1-x}Tb_xAl_2$, which in turn, will affect the nature of the spin reorientation transitions. The initial addition of Tb in $Ho_{1-x}Tb_xAl_2$ modifies the free energy of $HoAl_2$ stabilizing the easy direction along the [100] direction, and hence, no first order transition is observed in the $Ho_{1-x}Tb_xAl_2$ alloys with $x = 0.05$ and 0.07. As additional Tb is added to the system, the free energies with H_{ex} along different directions are further modified, and since [111] is the easy magnetization direction of $TbAl_2$ at all temperatures, the [111] direction becomes the dominant easy direction of $Ho_{1-x}Tb_xAl_2$ ($x > 0.07$) in the high temperature region. Hence the first order transition reappears for $x > 0.07$ and strengthens up to $x = 0.4$. As x exceeds 0.6, the [111] direction dominates at all temperatures as the easy magnetization direction and therefore no spin reorientation transition is observed in the $Ho_{1-x}Tb_xAl_2$ alloys for $x > 0.6$.

Figure 3 shows the variation of T_{SR} and T_C of $Ho_{1-x}Tb_xAl_2$ as a function of Tb concentration (x). T_C increases nearly linearly with increasing x while T_{SR} first jumps when x = 0.05, but when x exceeds 0.05, T_{SR} decreases nearly linearly with increasing x. The increase of T_C with increasing Tb concentration is due to the exchange of Tb^{3+} (quantified by the de Gennes factor of 0.667) being higher than the exchange of Ho^{3+} (de Gennes factor of 0.286). The decrease of T_{SR}, with increasing Tb concentration may also be attributed to the same reason. This is because with increasing Tb concentration the exchange energy in the $Ho_{1-x}Tb_xAl_2$ system becomes greater than the anisotropy energy associated with the spin reorientation transition. The decrease of spin reorientation transition temperature with increasing exchange energy is also observed in $RFe_{11}Ti$ systems.[25]

Figure 4 shows the C_P data of $HoAl_2$ measured at various magnetic fields. A minor suppression of the sharp peak upon the application of 5 kOe is clear in the figure. For a magnetic field of > 30 kOe the peak appears to be suppressed completely, while shifting to lower temperatures (see inset of Fig. 4). As also seen in Fig. 4, the anomaly at T_C broadens considerably with increasing magnetic field.

The field dependence of the C_P data for the $Ho_{1-x}Tb_xAl_2$ alloy with x = 0.10 are shown in Fig.5. Compared to pure $HoAl_2$, the first order heat capacity anomaly is fairly weak. The peak is significantly suppressed when a field of 5 kOe is applied, and it nearly disappears for a magnetic field of 10 kOe (see inset of Fig.5 for clarity). It is noted, that the high

magnetic field (larger than 10 kOe) anomalies observed in the C_P data of $HoAl_2$ are not observed in case of the $Ho_{1-x}Tb_xAl_2$ alloy with x = 0.10.

The C_P data of the $Ho_{1-x}Tb_xAl_2$ alloys with x = 0.25 and x = 0.40, measured at various magnetic fields, are shown in Fig. 6 and Fig. 7, respectively. The first order anomaly in the alloy with x = 0.25 is stronger than the anomaly observed in the alloy with x = 0.10. At a magnetic field of 5 kOe, the first order anomaly is only weakly affected. The anomaly is still visible when a field of 10 kOe is applied (see inset of Fig.6). When a magnetic field of 20 kOe is applied the first order anomaly is no longer observed in the C_P data of the $Ho_{1-x}Tb_xAl_2$ alloy with x = 0.25, transforming into a broad and weak enhancement of the heat capacity below the zero magnetic field T_{SR}. The behaviors observed in the C_P data of $Ho_{1-x}Tb_xAl_2$ alloy with x = 0.25 and x = 0.40 are similar, with the exception that the first order anomaly at 10 kOe field is stronger in the alloy with x = 0.4, and even at 20 kOe the anomaly is still visible in this alloy (see inset of Fig. 7).

Although the first order anomalies observed in the zero magnetic field C_P data are similar for $HoAl_2$ and $Ho_{1-x}Tb_xAl_2$ alloys ($x \geq 0.1$), an interesting difference concerning the nature of the transitions is noticed in the C_P data measured in the presence of magnetic fields. As shown in Fig.4, the transition in $HoAl_2$ shifts to lower temperatures with increasing magnetic fields, whereas the transition in $Ho_{1-x}Tb_xAl_2$ alloys ($x \geq 0.1$) shifts to higher temperatures with increasing magnetic fields (see insets of Fig.6 and Fig.7). This behavior indicates that interactions responsible for the first order anomalies are different for $HoAl_2$ and $Ho_{1-x}Tb_xAl_2$ alloys ($x \geq 0.05$). This conclusion is also supported by the

behavior shown in Fig. 1, where the partial replacement of Ho by only 5% Tb in $Ho_{1-x}Tb_xAl_2$ results in the disappearance of the first order peak and the emergence of a weak anomaly at a higher temperature.

In Fig. 8 we show the temperature variation of magnetization, M(T), of several $Ho_{1-x}Tb_xAl_2$ alloys measured in a magnetic field of 100 Oe in the vicinity of the spin reorientation transition. The M(T) data of $HoAl_2$ (Fig. 8a) show an increase of magnetization with increasing temperature until it drops in the vicinity of the spin reorientation transition at ~20 K. The M(T) data for the $Ho_{1-x}Tb_xAl_2$ alloy with x = 0.05, exhibit a weak slope of change at ~29 K, which is consistent with the weak anomaly seen in the C_P data of the alloy (see Fig. 1b). For the alloys with x = 0.25 a step like increase in magnetization is observed at ~20 K in the M(T) data (Fig. 8c). The same is observed in the alloys with x = 0.40. Different behaviors seen in the M(T) data further demonstrate that the magnetic interactions governing the first order transition in pure $HoAl_2$ are different from the interactions responsible for the transitions in $Ho_{1-x}Tb_xAl_2$ alloys when $x > 0.07$.

As shown in Fig. 2, the $Ho_{1-x}Tb_xAl_2$ alloy with x = 0.40 exhibits the first order C_P peak with the highest magnitude. In order to confirm the first order nature of this transition and explore the possibility of a structural transition in its vicinity, we have performed low temperature x-ray diffraction measurements on the sample with x = 0.40. Some of the XRD patterns along with the results of the Rietveld analysis are shown in Fig. 8 and Fig. 9. At all temperatures between 300 and 5 K, the alloy retains the $MgCu_2$ type cubic

structure. If there is any departure from the cubic symmetry, it is smaller than the sensitivity of our x-ray powder diffraction measurements, which can be estimated to be on the order of 20 parts per million.[21] A clear step-like anomaly in the lattice parameter is observed in the vicinity of the spin reorientation transition temperature (~ 16 K), which confirms the presence of volume discontinuity, and therefore, the first order nature of the spin reorientation transformation in this alloy (see Fig. 9). Similar to $Er_{0.75}Tb_{0.25}Al_2$[6] and $Er_{0.75}Dy_{0.25}Al_2$,[4] the lattice constant decreases smoothly with decreasing temperature until T_C, below which a weak deviation is observed, which is associated with spontaneous magnetostriction upon ferromagnetic ordering of the material.

CONCLUSIONS

A series of pseudo-binary $Ho_{1-x}Tb_xAl_2$ alloys have been studied using heat capacity and temperature-dependent x-ray powder diffraction measurements. The first order spin reorientation transition observed in pure $HoAl_2$, disappears for $x = 0.05$ in $Ho_{1-x}Tb_xAl_2$. As Tb concentration increases further, a different anomaly appears in the heat capacity data, which simultaneously gets stronger and shifts to lower temperatures with increasing Tb concentration. For $x = 0.25$, the heat capacity anomaly is very similar to the first order anomaly observed in pure $HoAl_2$ and the anomalies in both alloys are observed almost at the same temperature. Although, the thermodynamic nature of the anomalies appear similar in the heat capacity data obtained at zero magnetic fields, the field dependence of the heat capacities shows that the first order anomalies in $HoAl_2$ and $Ho_{1-x}Tb_xAl_2$ are different. The anomalies observed in the $Ho_{1-x}Tb_xAl_2$ ($x \geq 0.05$) alloys are believed to be

the result of competing anisotropy that arises due to the differences in the Stevens' factors of Ho and Tb, especially the fourth order parameters that are opposite in sign for Ho and Tb. No structural transformation accompanying the first order spin reorientation transition could be detected using temperature-dependent X-ray powder diffraction data measured for the alloy with x = 0.40; the volume discontinuity observed at T_{SR} confirms the first order nature of the spin reorientation trtansition.

ACKNOWLEDGEMENTS

This work was supported by the U.S. Department of Energy, Office of Basic Energy Science, Division of Materials Sciences and Engineering. The research was performed at the Ames Laboratory. Ames Laboratory is operated for the U.S. Department of Energy by Iowa State University under Contract No. DE-AC02-07CH11358.

REFERENCES

FIGURE CAPTIONS

FIG. 1 (Color online). The heat capacities of $Ho_{1-x}Tb_xAl_2$ ($0 \leq x \leq 0.1$) measured in zero magnetic field. The inset in (b) shows the derivative of the heat capacity of the alloy with $x = 0.05$. The insets in (c) and (d) show the temperature regions in the vicinity of the spin reorientation transition.

FIG. 2 (Color online). The heat capacities of $Ho_{1-x}Tb_xAl_2$ ($0.15 \leq x \leq 0.75$) measured in zero magnetic field.

FIG. 3 (Color online). Spin reorientation transition temperatures, T_{SR}, and Curie temperatures, T_C, of $Ho_{1-x}Tb_xAl_2$ as functions of Tb concentration.

FIG. 4 (Color online). Heat capacity of $Ho_{1-x}Tb_xAl_2$ ($x = 0.0$) as a function of temperature measured at different magnetic fields. The inset shows the temperature region in the vicinity of the spin reorientation transition.

FIG. 5 (Color online). Heat capacity of $Ho_{1-x}Tb_xAl_2$ ($x = 0.10$) as a function of temperature measured at different magnetic fields. The inset shows the temperature region in the vicinity of the spin reorientation transition.

FIG. 6 (Color online). Heat capacity of $Ho_{1-x}Tb_xAl_2$ (x = 0.25) as a function of temperature measured at different magnetic fields. The inset shows the temperature region in the vicinity of the spin reorientation transition.

FIG. 7 (Color online). Heat capacity of $Ho_{1-x}Tb_xAl_2$ (x = 0.40) as a function of temperature measured at different magnetic fields. The inset shows the temperature region in the vicinity of the spin reorientation transition.

FIG. 8 (Color online). Observed (symbols) and calculated (line drawn through the symbols) X-ray powder diffraction patterns of $Ho_{1-x}Tb_xAl_2$ (x = 0.4), measured at different temperatures (below T_{SR}, between T_{SR} and T_C, and above T_C). The difference $Y_{obs} - Y_{calc}$ is shown at the bottom of the plot. Vertical bars under the patterns indicate calculated positions of Bragg peaks in the cubic $MgCu_2$-type structure.

FIG. 9 (Color online). Temperature variation of the lattice parameter of $Ho_{1-x}Tb_xAl_2$ (x = 0.4). Error bars are smaller than the size of the data points in the figure.

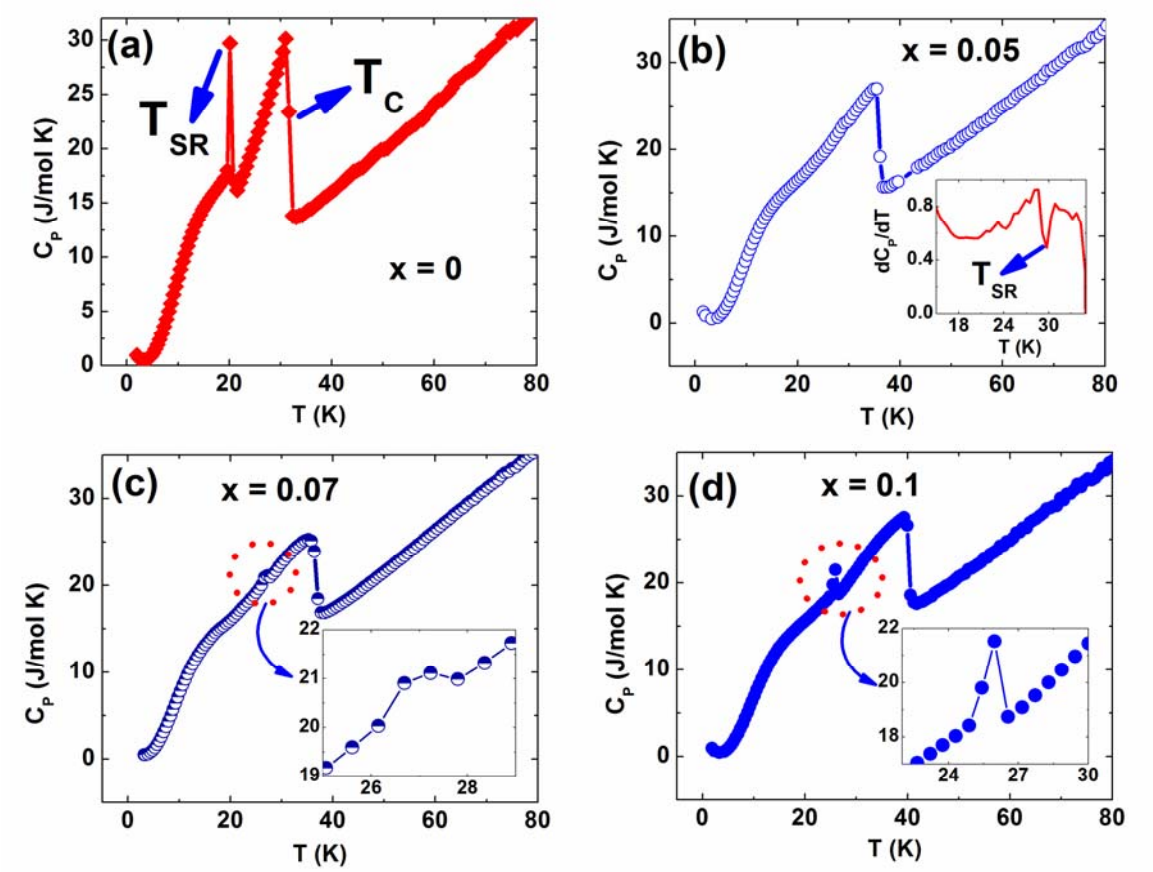

FIG. 1 (Color online). The heat capacities of $Ho_{1-x}Tb_xAl_2$ ($0 \leq x \leq 0.1$) measured in zero magnetic field. The inset in (b) shows the derivative of the heat capacity of the alloy with x = 0.05. The insets in (c) and (d) show the temperature regions in the vicinity of the spin reorientation transition.

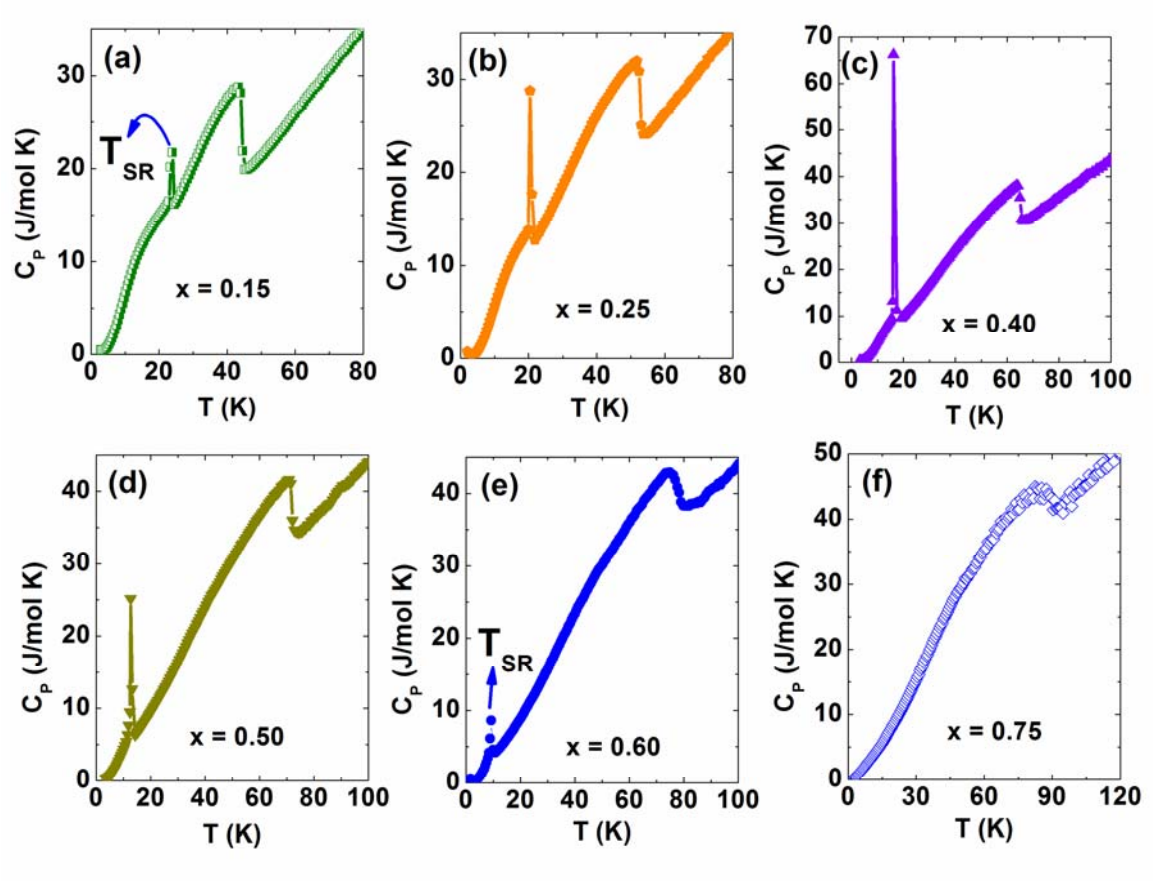

FIG. 2 (Color online). The heat capacities of $Ho_{1-x}Tb_xAl_2$ ($0.15 \leq x \leq 0.75$) measured in zero magnetic field.

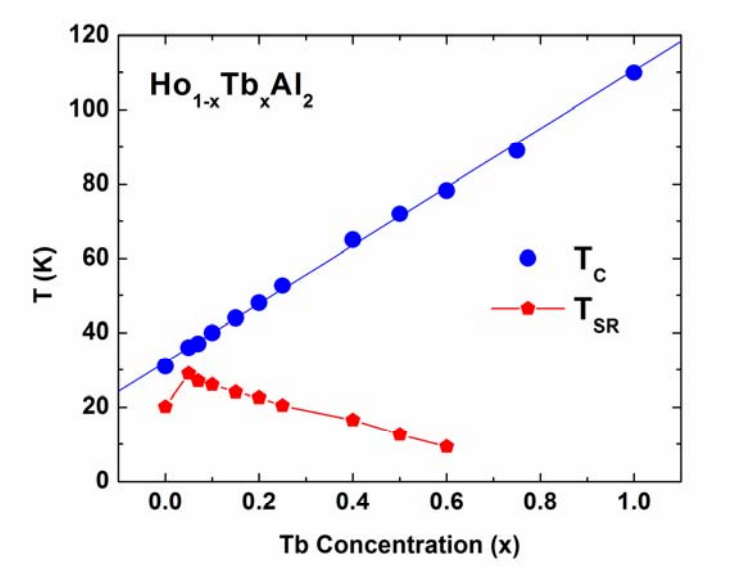

FIG. 3 (Color online). Spin reorientation transition temperatures, T_{SR}, and Curie temperatures, T_C, of $Ho_{1-x}Tb_xAl_2$ as functions of Tb concentration.

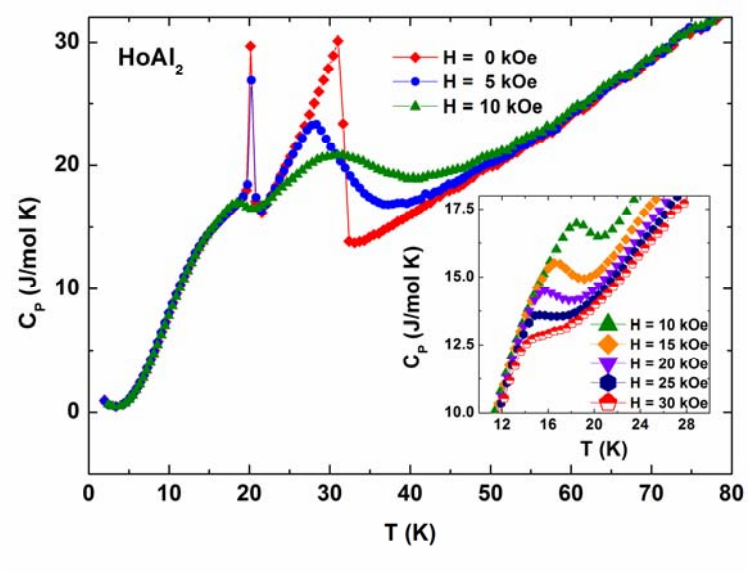

FIG. 4 (Color online). Heat capacity of $Ho_{1-x}Tb_xAl_2$ (x = 0.0) as a function of temperature measured at different magnetic fields. The inset shows the temperature region in the vicinity of the spin reorientation transition.

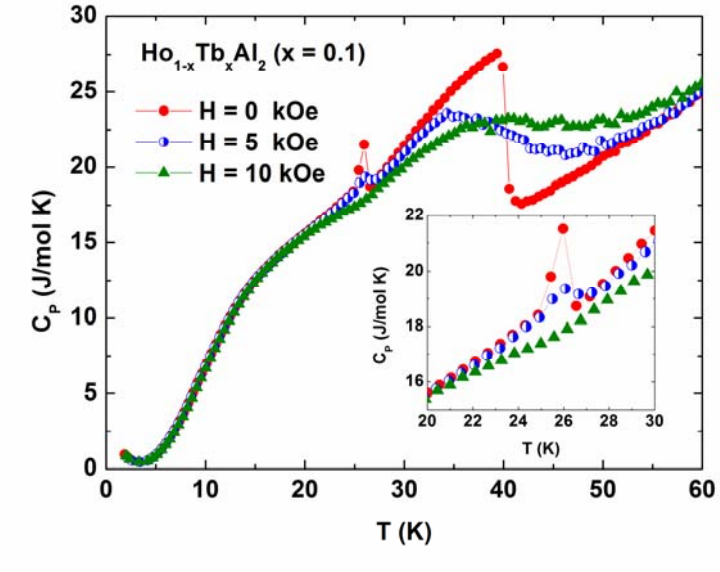

FIG. 5 (Color online). Heat capacity of $Ho_{1-x}Tb_xAl_2$ (x = 0.10) as a function of temperature measured at different magnetic fields. The inset shows the temperature region in the vicinity of the spin reorientation transition.

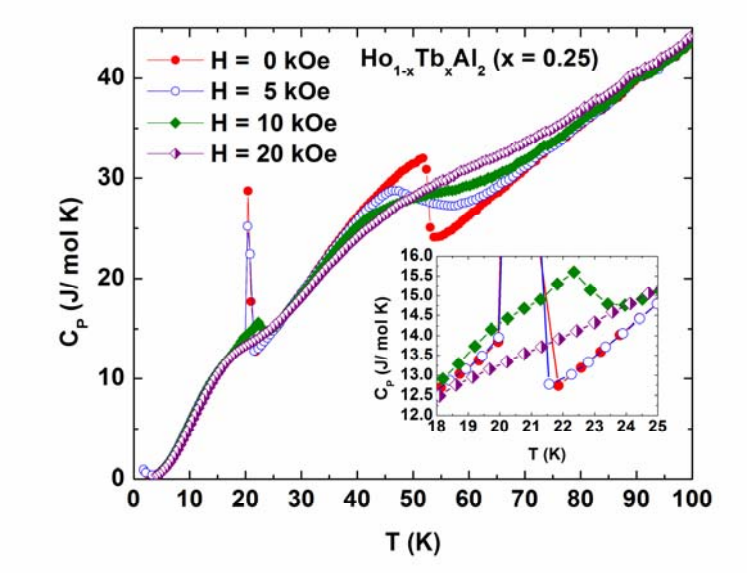

FIG. 6 (Color online). Heat capacity of $Ho_{1-x}Tb_xAl_2$ (x = 0.25) as a function of temperature measured at different magnetic fields. The inset shows the temperature region in the vicinity of the spin reorientation transition.

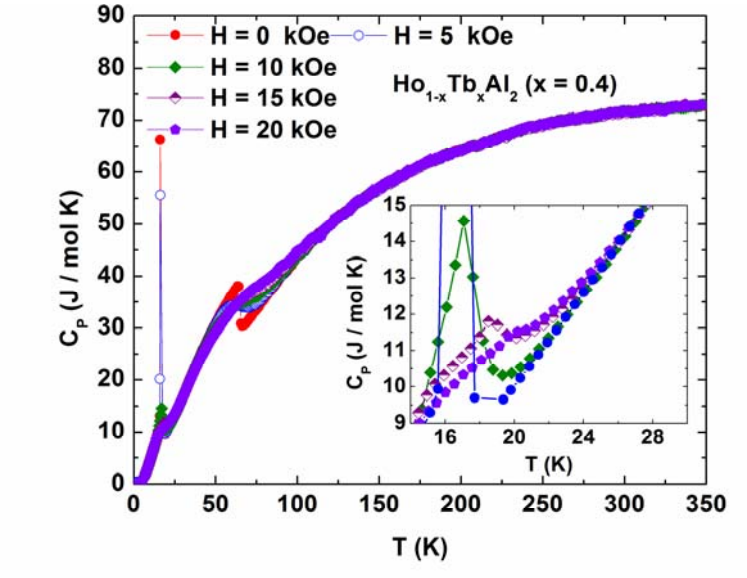

FIG. 7 (Color online). Heat capacity of $Ho_{1-x}Tb_xAl_2$ (x = 0.40) as a function of temperature measured at different magnetic fields. The inset shows the temperature region in the vicinity of the spin reorientation transition.

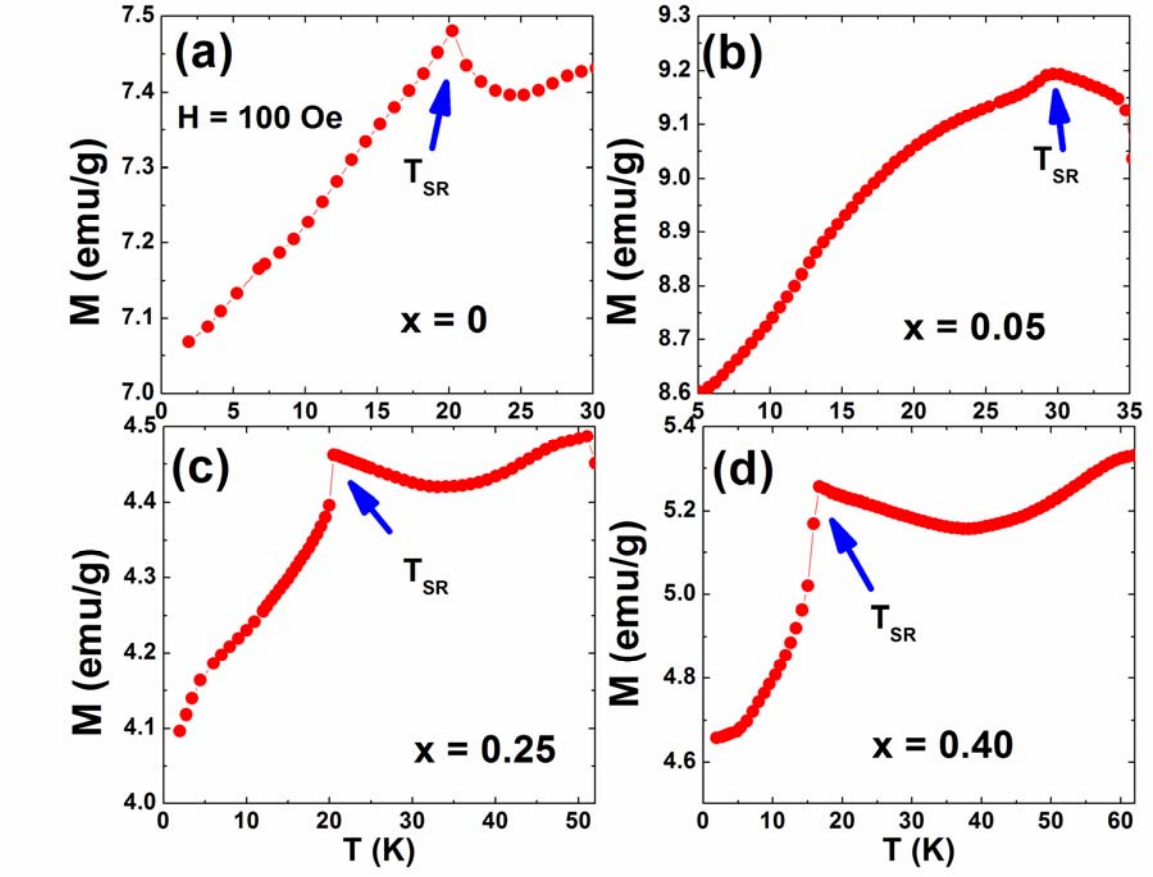

FIG. 8 (Color online). Temperature variation of magnetization of $Ho_{1-x}Tb_xAl_2$ measured at magnetic fields of 100 Oe.

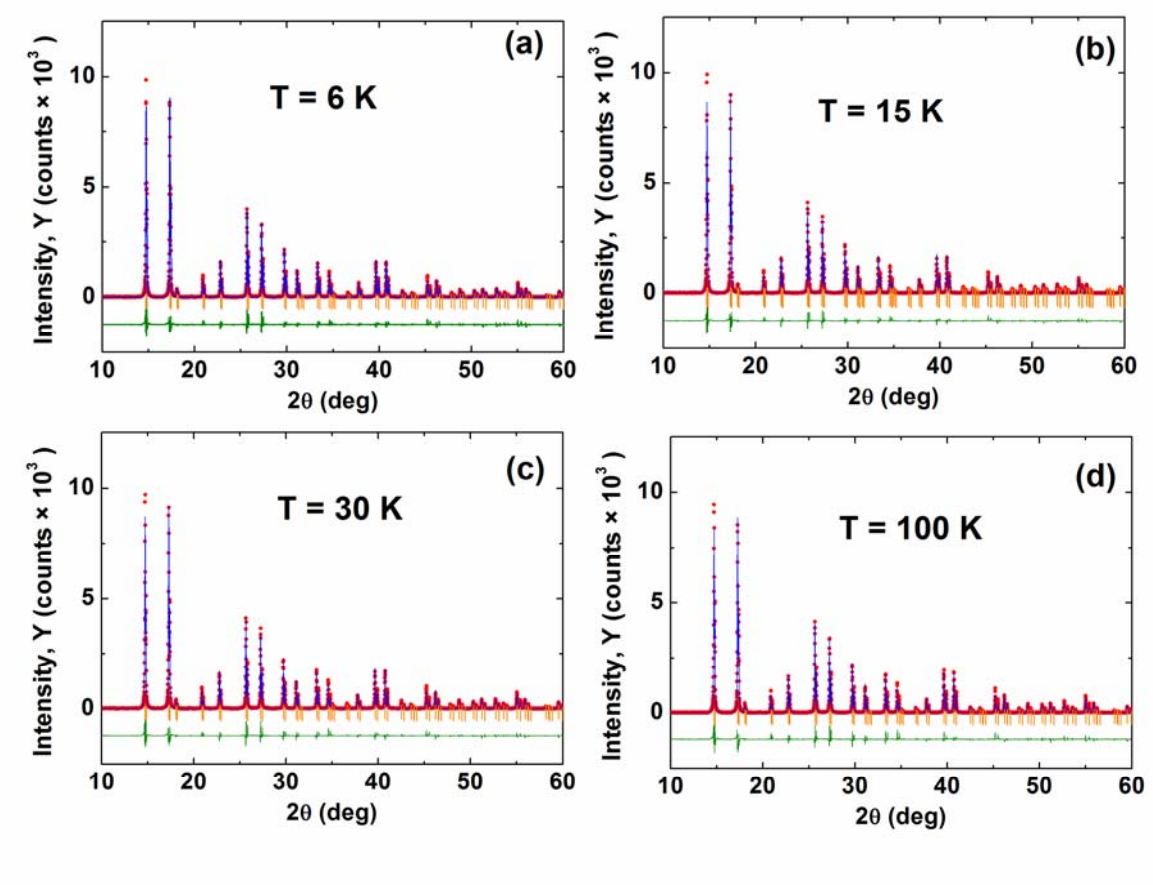

FIG. 8 (Color online). Observed (symbols) and calculated (line drawn through the symbols) X-ray powder diffraction patterns of $Ho_{1-x}Tb_xAl_2$ (x = 0.4), measured at different temperatures (below T_{SR}, between T_{SR} and T_C, and above T_C). The difference $Y_{obs} - Y_{calc}$ is shown at the bottom of the plots. Vertical bars under the patterns indicate calculated positions of Bragg peaks in the cubic $MgCu_2$-type structure.

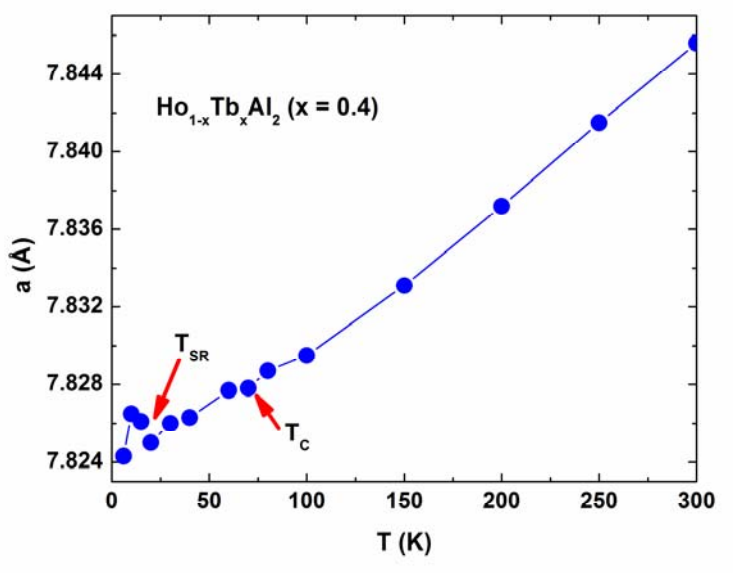

FIG. 9 (Color online). Temperature variation of the lattice parameter of $Ho_{1-x}Tb_xAl_2$ (x = 0.4). Error bars are smaller than the size of the data points in the figure.

[1] K. W. H. Stevens, Proc. Phys. Soc. LXV, **A65**, 209-215 (1952).

[2] Nguyen Huu Duc, in *Handbook on the Physics and Chemistry of Rare Earths*, edited by K. A. Gschneidner, Jr., L. Eyring and G. H. Lander (North-Holland, Amsterdam, 2001), Vol. **32**, Chap. 205, p.10.

[3] A. L. Lima, K. A. Gschneidner, Jr., V. K. Pecharsky, and A. O. Pecharsky, Phys. Rev. B **68**, 134409 (2003).

[4] R. Nirmala, Ya. Mudryk, V. K. Pecharsky and K. A. Gschneidner, Jr., Phys. Rev. B **76**, 014407 (2007).

[5] Mahmud Khan, V. K. Pecharsky and K. A. Gschneidner, Jr., Phys. Rev. B **80**, 224408 (2009).

[6] Mahmud Khan, Ya. Mudryk, D. Paudyal, K. A. Gschneidner, Jr. and V. K. Pecharsky, Phys. Rev. B **82**, 064421 (2010).

[7] Mahmud Khan, D. Paudyal, Ya. Mudryk, K. A. Gschneidner, Jr. and V. K. Pecharsky, Phys. Rev. B **83**, 134437 (2011).

[8] P. Morin, J. Pierre, and J. Chaussy, Phys. Status Solidi A **24**, 425 (1974).

[9] B. Barbara, M.F. Rossignol, and J.X. Boucherle, Phys. Lett. **55A**, 321 (1975).

[10] B. Barbara, J.X. Boucherle, M.F. Rossignol and J. Schweizer, Physica B, **86–88**, 83 (1977).

[11] W. Schelp, A. Leson, W. Drewes, H. Purwins, and H. Grimm, Z. Phys. B: Condens. Matter **51**, 41 (1983).

[12] C.M. Williams, N.C. Koon and B.N. Das J. Appl. Phys., **50**, 1669 (1979).

[13] M. R. Ibarra, E. W. Lee, A. del Moral, and O. Moze, Solid State Commun. **53**, 183 (1985).

[14] B. Daudin and E. Bonjour, C. R. Seanc. Acad. Sci. Ser. II (France) **295**, 535 (1982).

[15] T. Inoue, S. G. Sankar, and R. S. Craig, J. Appl. Phys. **49**, 1951 (1978).

[16] T.W. Hill, W.E. Wallace, R.S. Craig and T. Inoue, J. Solid State Chem., **8**, 364 (1973).

[17] A. H. Millhouse, H. G. Purwins, and E. Walker, Solid St. Commun., **11**, 707 (1972).

[18] S.G. Sankar, S.K. Malik, and V.U.S. Rao, J. Solid State Chem. **18**, 303 (1976).

[19] Materials Preparation Center, The Ames Laboratory U.S. Department of Energy, Ames, IA, USA, www.mpc.ameslab.gov.

[20] B. Hunter, Rietica-A Visual Rietveld Program, International Union of Crystallography Commission on Powder Diffraction Newsletter No. 20, (Summer, 1998) http://www.rietica.org.

[21] V.K. Pecharsky and P.Y.U. Zavalij, *Fundamentals of powder diffraction and structural characterization of materials,* Kluwer Academic Publisher, Boston (2009).

[22] A. P. Holm, V. K. Pecharsky, K. A. Gschneidner, Jr., R. Rink, and M. N. Jirmanus Rev. Sci. Instrum. 75, 1081 (2004).

[23] Ya. Mudryk, A. P. Holm, K. A. Gschneidner, Jr., and V. K. Pecharsky, Phys. Rev. B **72**, 064442 (2005).

[24] V. K. Pecharsky, J. O. Moorman, and K. A. Gschneidner, Jr., Rev. Sci. Instrum. **68**, 4196 (1997).

[25] X.C. Kou, T.S. Zhao, R. Grossinger, H.R. Kirchmayr, X. Li, and F.R. de Boer, Phys. Rev. B **47**, 3231 (1993).